

Diameter-Dependent Solubility of Single-Walled Carbon Nanotubes

Juan G. Duque,^{†,‡,§,⊥,‡} A. Nicholas G. Parra-Vasquez,^{†,‡,▽} Natnael Behabtu,^{†,‡} Micah J. Green,^{†,‡,○} Amanda L. Higginbotham,^{||,‡} B. Katherine Price,^{||,♦} Ashley D. Leonard,^{||} Howard K. Schmidt,^{†,‡,¶} Brahim Lounis,[⊥] James M. Tour,^{‡,||} Stephen K. Doorn,[§] Laurent Cognet,[⊥] and Matteo Pasquali^{†,‡,¶,||,*}

[†]Department of Chemical and Biomolecular Engineering, Rice University, 6100 Main Street, Houston, Texas 77005, [‡]The Smalley Institute for Nanoscale Science and Technology, Rice University, 6100 Main Street, Houston, Texas 77005, [§]Los Alamos National Laboratory, Physical Chemistry and Applied Spectroscopy (C-PCS) Group, Los Alamos, New Mexico 87544, [⊥]Centre de Physique Moléculaire Optique et Hertzienne, Université de Bordeaux and CNRS, 351 cours de la libération, Talence F-33405, France, and ^{||}Department of Chemistry, Rice University, 6100 Main Street, Houston, Texas 77005. [¶]Present address: Los Alamos National Laboratory, Los Alamos, NM 87544. [▽]Present address: Université de Bordeaux and CNRS, Talence, France. [○]Present address: Texas Tech University, Lubbock, TX 79409. [♦]Present address: Imperial College, London, U.K. [⊥]Present address: Saudi Aramco, EXPEC-Advanced Research Center, Dhahran, Saudi Arabia.

Single-walled carbon nanotubes (SWNTs) possess unique mechanical, optical, and electronic properties; these properties are best realized when they are dispersed as individuals.¹ However, the heterogeneity in length, diameter, and chirality as well as the strong van der Waals forces of the as-produced (hereafter referred to as raw) SWNT samples makes it difficult to obtain individualized SWNTs that retain their intrinsic properties in macroscopic applications.¹ Recent efforts have focused on obtaining suspensions of only a single type of SWNT. Specifically, separation of SWNTs by diameter has been of significant interest, because intrinsic SWNT properties depend strongly on the diameter.² For example, the strong luminescence of small diameter semiconducting SWNTs (diameter <0.7 nm) can be used to investigate exciton processes and exciton–phonon interactions which can potentially reveal novel information on unique optical and electronic properties of SWNTs.^{3–7} Moreover, small diameter SWNTs are particularly desirable for material reinforcement, selective chemistry, optoelectronics, and nanophotonics;^{1,2,8} however, only low concentrations of separated SWNT types have been obtained which greatly limits realization of their potential.²

While the construction of single molecular devices from SWNTs has been achieved,⁹ manipulating bulk samples into macroscopic entities with optimal properties remains a challenge. A common method to produce macroscopic structures from nanoparticles is self-assembly;¹⁰ in its simplest form, it consists of dissolving the nanoparti-

ABSTRACT We study the solubility and dispersibility of as-produced and purified HiPco single-walled carbon nanotubes (SWNTs). Variation in specific operating conditions of the HiPco process are found to lead to significant differences in the respective SWNT solubilities in oleum and surfactant suspensions. The diameter distributions of SWNTs dispersed in surfactant solutions are batch-dependent, as evidenced by luminescence and Raman spectroscopies, but are identical for metallic and semiconducting SWNTs within a batch. We thus find that small diameter SWNTs disperse at higher concentration in aqueous surfactants and dissolve at higher concentration in oleum than do large-diameter SWNTs. These results highlight the importance of controlling SWNT synthesis methods in order to optimize processes dependent on solubility, including macroscopic processing such as fiber spinning, material reinforcement, and films production, as well as for fundamental research in type selective chemistry, optoelectronics, and nanophotonics.

KEYWORDS: single-walled carbon nanotubes · solubility · solutions · dispersions · diameter

cles individually in a liquid and then manipulating the liquid to produce the desired macroscopic structure. In this respect, the strong van der Waals interactions between SWNT sidewalls have made dispersion in fluids very difficult. Successful techniques include covalent functionalization^{11,12} and reversible protonation *via* superacids.¹³ Alternatively, SWNTs can be individualized by sonication and stabilized against reaggregation by wrapping with surfactants,^{14–17} polymers,¹⁸ or DNA.^{19–22}

The dispersion of SWNTs as individuals in a liquid has allowed for a better understanding of their spectroscopic properties,^{14,23} thereby opening up research areas such as biosensing^{24,25} and targeted therapy for cancer treatment,²⁶ and allowed the development of self-assembly processes for producing SWNT films and fibers.^{27,28} Moreover, individual SWNTs in solution are more accessible for chemical manipulation, including sidewall

*Address correspondence to mp@rice.edu.

Received for review January 27, 2010 and accepted May 24, 2010.

Published online June 3, 2010.
10.1021/nn100170f

© 2010 American Chemical Society

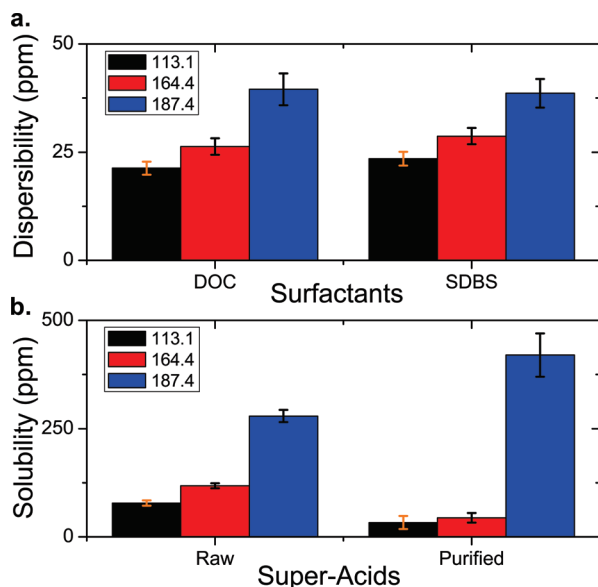


Figure 1. Dispersibility of raw HiPco SWNTs in anionic surfactants (DOC and SDBS) (a) and the solubility of raw and purified HiPco SWNTs in oleum (b) for HiPco batches 187.4 (blue), 164.4 (red), and 113.1 (black).

functionalization^{11,12,29} and cutting.³⁰ Such manipulation is useful for incorporating SWNTs into high performance polymer composites.³¹

Even when a standardized SWNT dispersion technique is used, the dispersions yield highly variable results, primarily due to the broad range of available SWNT production techniques as well as batch-to-batch differences within the same production process. For example, in HiPco production,³² the SWNT characteristics depend on the reactor parameters:³³ the CO reactant pressure affects the diameter distribution and the catalyst flow rate affects the diameter and length distribution as well as the fraction of fullerenes and amorphous carbon impurities.³³

We studied the dispersibility in surfactants and the solubility in oleum (H_2SO_4 , 20% free SO_3) of three batches of raw-HiPco SWNTs and found large variations in solubility, dispersibility, and diameter distribution in all batches. By measuring the diameter distributions of the different batches, we found that smaller diameter SWNTs have higher solubility and dispersibility. Moreover, we observed striking variation in the solubility between raw and purified SWNTs.³⁴ These results highlight the importance of controlling the synthesis and postprocessing methods such that SWNTs with target properties may be obtained. Applications that require high concentrations of individually dispersed SWNTs such as production of thin films, SWNT functionalization, and cutting are especially sensitive to these variations.

RESULTS AND DISCUSSION

Three different HiPco batches were selected for this study (113.1, 164.4, and 187.4). These batches were pro-

duced using different reactor parameters including catalyst concentration, gas flow rate, and reactor design (see Experimental Section).

Batch-Dependent Solubility of HiPco SWNTs. Both the solubility in oleum³⁴ (H_2SO_4 , 20% free SO_3) and the dispersibility in two aqueous anionic surfactants¹⁴—dodecylbenzenesulfonic acid sodium salt (SDBS) and sodium deoxycholate (DOC)—were studied (see Experimental Section). The concentration of SWNTs in the different dispersions was determined from the extinction coefficient found by UV–vis–NIR absorbance similar to previous reports.³⁵ The dispersibility in surfactant-stabilized aqueous suspensions was determined for raw-SWNTs. In oleum, the solubility was measured for both raw and purified SWNTs (see Experimental Section) in order to assess the effects purification procedures can have on solubility.

Figure 1a,b shows that the three batches have significantly different solubilities. In both oleum and surfactant suspensions, batch 187.4 had the highest raw solubility (279 and ~39 parts-per-million (ppm, by mass), respectively) while batch 113.1 had the lowest (78 and ~22 ppm, respectively). A similar batch-dependence for solubility of purified SWNTs in oleum is also observed (Figure 1b), but the purification method affected the solubility in oleum for each of the batches differently (see also Supporting Information). Solubility is increased for batch 187.4 in the purified case compared to the raw result, while it is decreased for the other two batches. Although this highlights the importance of controlling all processes used to generate the final SWNT product, we focus the remainder of our analysis on the raw-SWNTs in order to better understand which of their properties affect solubility.

SWNT solubility has been predicted to vary with length,³⁶ but the average length produced by the HiPco process (0.8–1.3 μm ³³) is insufficient to account for the substantial solubility differences reported here.^{36,37} Differences in SWNT diameter distribution may also affect their solubility and dispersibility because intertube interactions (dominated by van der Waals forces), surfactant conformation, and tube protonation all depend on diameter.^{36,38–41} So far, it has been assumed that the mean diameter of HiPco SWNTs is ~1 nm,³³ with small batch to batch variations (± 0.05 nm). Previously, HiPco diameter distributions were obtained by transmission electron microscopy (TEM); however, this is not a “bulk” technique and the results are limited to only a few images taken of a given sample. Here we measure more accurately the diameter distribution in our samples by combining several complementary spectroscopic techniques (Raman, absorbance, luminescence), to avoid any potential bias intrinsic in a single technique.

Raman, in particular, allows the verification that metallic and semiconductor diameter distributions are similar.^{42–45} The result is the demonstration of a strong

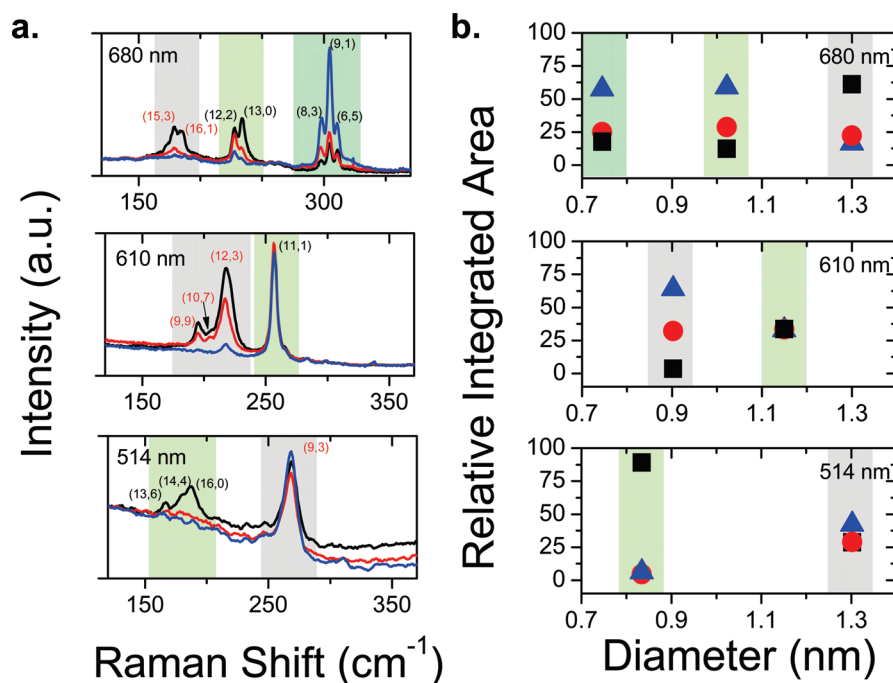


Figure 2. (a) Radial breathing mode (RBM) peaks of HiPco 187.4 (blue trace), 164.4 (red trace), and 113.1 (black trace) in 1 wt % DOC at different excitation wavelengths (680, 610, and 514 nm). Metallic SWNT (n,m) indices are in red and denoted by a gray box and semiconductors in black and denoted by a green box. (b) Relative integrated area of the RBMs at 680, 610, and 514 nm excitation wavelengths. The relative integrated area was determined for each SWNT family denoted by the green and gray box (see Supporting Information for more details). The diameters were determined by taking the mean diameter of each population (family) of SWNTs found in the corresponding Raman RBM spectra. The colors of the symbols in Figure 2b correspond to the matching traces of Figure 2a.

correlation between diameter distribution and solubility, in support of our hypothesis that the observed differences in solubility and dispersibility are diameter-induced.

Spectroscopic Demonstration of Diameter-Dependent Solubilities. The different batches of SWNTs were studied spectroscopically in order to test our hypothesis that the differences in solubility and dispersibility are diameter induced. Resonant Raman spectroscopy, UV-vis-nIR absorbance, and luminescence were performed on individually suspended surfactant-wrapped SWNTs prepared using a procedure modified from ref 14. All spectroscopic characterizations were performed on raw-SWNT aqueous dispersions at ~ 10 ppm (see Experimental Section).

Raman Spectroscopy. Examination of the radial breathing mode (RBM) region of the Raman spectra reveals that the different batches have different diameter distributions both for metallic and semiconducting species.^{23,43–48} The strong SWNT RBM resonances (between 497–850 nm excitation wavelength) allow assignment of 55 different (n,m) chiralities within the three studied batches,^{43–48} grouped in 12 semiconducting and 7 metallic families (formed by $2n + m = \text{constant}$, assigned SWNTs can be found in Table S.1 in the Supporting Information) with diameters ranging from 0.62 to 1.564 nm. Figure 2a shows a series of RBM peaks and their respective (n,m) assignment as a function of excitation wavelength^{43–48} for batches 187.4 (blue

trace), 164.4 (red trace), and 113.1 (black trace) containing SWNTs dispersed in DOC. By performing resonant Raman spectroscopy with excitation at 680 nm, three families are selected: two semiconducting ($2n + m = 19$ and 26) and one metallic ($2n + m = 33$) (Figure 2a). In batch 187.4, the predominant peak is found to be from the small diameter family 19 and corresponds to the (9,1) tube ($d \approx 0.782$ nm). In contrast, batch 113.1 contains predominantly larger diameter families 26 and 33, corresponding to (13,0) tubes ($d \approx 1.043$ nm) and (16,1) tubes ($d \approx 1.313$ nm), respectively. Comparison of the relative integrated areas of specific RBMs over a given frequency range can provide a more quantitative measure of how the relative population abundance of a given diameter range changes between specific SWNT batches (Figure S.1 in the Supporting Information).⁴⁹ The relative integrated area of the populations in Figure 2b show that in batch 187.4 there is a greater population of smaller diameter tubes, while in batch 113.1 there is a greater population of large diameter tubes. For the other two excitation wavelengths (610 and 514 nm) shown in Figure 2a, there are two regions selected: ~ 260 cm⁻¹ ($d \approx 0.9$ nm) and ~ 200 cm⁻¹ ($d \approx 1.2$ nm). These two wavelengths were selected to better illustrate the different diameter distribution behavior for both semiconducting and metallic species; 610 nm is in resonance with smaller diameter semiconductors and larger diameter metallics (E_{22} and M_{11} transitions, respectively), while 514 nm is in resonance with the E_{33}

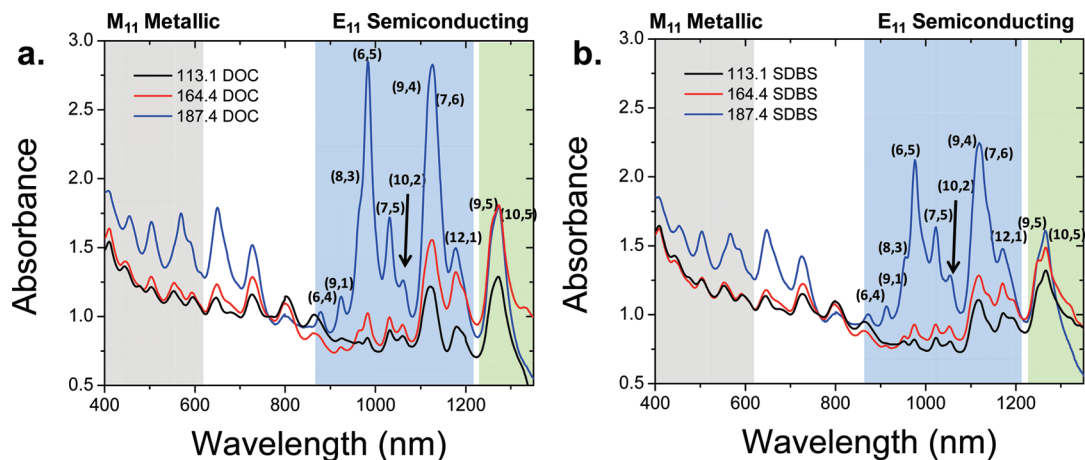


Figure 3. (a–b) UV–vis–nIR absorbance of raw-SWNTs from HiPco batches 187.4 (blue trace), 164.4 (red trace), and 113.1 (black trace) dispersed in DOC (a) and SDBS (b) surfactants. The blue (SWNTs $d \leq 1$ nm) and green (SWNTs $d \geq 1$ nm) regions are associated with different diameters of SWNTs. The gray region represents the M_{11} transitions of the metallic SWNTs.

transitions of the large diameter semiconductors and the M_{11} transitions of the small diameter metallics (Figure S.2e in the Supporting Information).^{6,43–47} The RBM intensities of small diameter SWNTs ($d \approx 0.9$ nm), corresponding to the (11,1) semiconducting SWNT (610 nm) and the (9,3) metallic SWNT (514 nm), are mainly independent of the batches (Figure 2b). In contrast, batch 113.1 contains a higher proportion of large diameter metallic (610 nm) and semiconducting (514 nm) SWNTs than the two other batches.

For further comparison of the RBM response expected from batches composed of predominantly large diameter SWNTs, we compare the RBM spectra of HiPco SWNTs to that obtained with laser oven SWNTs (Carbon Solutions, Inc., batch no. 02-304). We find that the laser oven SWNTs have a high proportion of larger diameter tubes, with the mean diameter centered at ~ 1.4 nm (Supporting Information Figure S.3, 633 and 514 nm excitation).^{23,42} The RBM region of the laser oven SWNTs displays peaks at lower frequencies (~ 200 cm^{-1}), like HiPco batch 113.1, confirming that the observed peaks are from the E_{33} resonance of large diameter semiconducting SWNTs (Supporting Information Figure S.3). No significant RBM peaks corresponding to small diameter SWNTs were observed in the laser oven samples; moreover, no fluorescence signal in the near-IR region (900–1400 nm) using 660 or 785 nm excitation wavelength was obtained from laser oven SWNTs.

Importantly, Raman spectra taken on all batches before ultracentrifugation gave comparable results, indicating that ultracentrifugation does not selectively deplete any specific type or diameter in our dispersion conditions. SDBS suspensions gave qualitatively similar results (Supporting Information Figure S.2b). Moreover, the different observations discussed in Figure 2 are consistent with data taken across all excitation wave-

lengths, as shown in Supporting Information Figure S.2a–d.

Absorbance and Luminescence Spectroscopy. UV–vis–nIR absorbance spectra and 2D-contour luminescence excitation plots corroborate the different diameter distributions observed by Raman. In Figure 3a,b, the absorption peaks of semiconductors (E_{11} in the range 900–1400 nm) can be separated into two regions: a small diameter (< 1 nm) region (900–1250 nm, denoted by the blue box) and a large diameter region (1250–1400 nm, denoted by the green box). In batch 187.4 (blue trace), the peaks in the small diameter region are more intense and narrower than in batches 164.4 (red trace) and batch 113.1 (black trace). For all three batches, the large diameter peaks^{23,42} do not exhibit significant differences.

In Figure 4a,b, 2D-contour luminescence plots also confirm that batch 187.4 contains predominantly smaller diameter semiconductors, with the (6,5) peaks being more intense ($d = 0.757$ nm), than found in 164.4 and 113.1. Accordingly, batches 164.4 and 113.1 show significantly more intense signals for large diameter SWNTs ($d > 0.9$ nm), that is, for (8,6), (9,4), (11,3), (9,5), (10,3), (8,7), (9,7), and (10,5) tubes. Normalizing the intensity of the 2D-contour plots by the intensity of the (6,5) SWNT shows unequivocally the distinct differences in diameter distribution of semiconducting SWNTs in the three batches (Supporting Information Figure S.4b). To quantify the relative abundance and mean diameter of the distribution of semiconducting SWNTs in each batch, a histogram of diameter distribution was built from these luminescence measurements (see Supporting Information Figure S.4a for more details).⁴² Batch 187.4 shows the narrowest diameter distribution with a mean diameter of 0.78 nm, close to the diameter of a (6,5) SWNT. Batches 164.4 and 113.1 have a wider distribution with larger mean diameters of 0.83 and 1.03 nm, respectively.

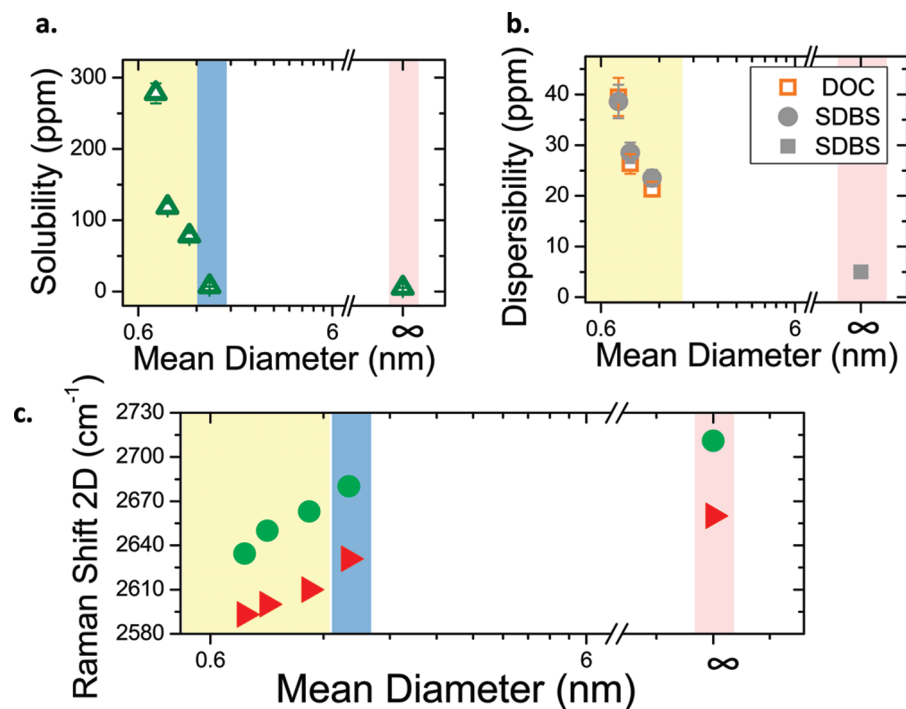


Figure 5. Diameter dependence of the (a) solubility of raw HiPco SWNTs (yellow region in all plots), laser oven SWNTs (blue region in all plots), and graphite (pink region in all plots) in oleum as a function of diameter, and (b) dispersibility of raw HiPco SWNTs in DOC (orange open squares) and SDBS (gray circles) compared to exfoliated graphene dispersibility data (gray square, red region) extracted from Figure 2 of ref 47. (c) Raman shift of the 2D peak as a function of mean diameter using 514 (green dots) and 633 nm (red triangles) excitation wavelengths. We assigned graphite to have a diameter of ∞ to represent a flat surface.

been seen by McDonald *et al.*⁶⁰ and Niyogi *et al.*⁶¹ which show SDS interacts more strongly with small diameter SWNTs. In contrast, recent separations results suggest DOC interacts more strongly with large diameter SWNTs.⁶² Further experimentation on diameter-selected SWNT samples will be valuable in elucidating how the specific details of surfactant interaction contribute to dispersibility.

While entropic factors and van der Waals interactions contribute to the diameter dependence of solubility in oleum, they do not completely explain the increased solubilities and strong diameter-dependences observed with oleum. The solubility of SWNTs and fullerenes in strong acids depends on the degree of protonation of their sidewalls.^{34,51} Stronger acids induce stronger protonation and, hence, are better solvents.^{34,51} For a given acid, solubility is related to curvature in fullerenes; smaller fullerenes have higher curvature and hence higher protonation and solubility.^{52,53} We hypothesize that this mechanism can be generalized to other structures of sp^2 carbon. Sharper curvature yields higher strain on the sp^2 -hybridized carbon structure. This strain can be relieved by removing electrons from the structure, or protonating the SWNT sidewalls. Therefore, highly strained, small-diameter SWNTs should protonate more readily than large-diameter SWNTs. To quantify the degree of strain for a given SWNT material, we compared the shift in the location of the 2D peak in the Raman spectra, which downshifts

to lower values for higher strains.^{54,55} Figure 5c shows that the 2D peak, for a given excitation wavelength, upshifts, indicating less strain as the diameter increases until a plateau is reached for large diameters (>1.4 nm). Expectedly, this correlates directly with a decrease in solubility to minimal values for large-diameter SWNTs (>1.4 nm). Ramesh *et al.* (2007) used similar observations to separate tubes by diameter by washing a SWNT sample with progressively stronger superacids.⁵³

Although there are similarities in the diameter-dependent trends in dispersibility in surfactants and oleum, their equilibrium behaviors are quite different. SWNT solutions in superacids are equilibrium phases that form spontaneously. Conversely, surfactant-stabilized suspensions of SWNTs in water are colloidal suspensions that are not in thermal equilibrium and must be prepared by intense mechanical shearing; therefore, the suspension concentration depends on processing conditions such as sonication time and intensity⁶³ as well as surfactant type and concentration. Therefore, results obtained from acid solutions and aqueous suspensions should be compared cautiously.

CONCLUSIONS

We have shown that, by controlling the reactor parameters, the HiPco process can yield batches with markedly different diameter distributions; such diameter differences affect the SWNT solubility in superacids and dispersibility in surfactants. Postprocessing of

batches, that is, purification, can also affect SWNT solubility and must be controlled. We have also shown that in oleum, the small-diameter SWNTs are more easily protonated and thus more soluble than larger ones. These results are important because of their implica-

tions for increasing the yield in single (n,m) SWNT-type separations. Furthermore, solubility and dispersibility are key parameters for macroscopic SWNT processing techniques including fiber spinning, material reinforcement, and thin-film production.

EXPERIMENTAL METHODS

Reactor Design. The overall design of the HiPco reactor has been described by Carver *et al.*,³³ the three batches used in this study (113.1, 164.4, and 187.4) were produced with different reactor subdesigns. Batch 113.1 was produced using the so-called “graphite blaster” design, with a water-cooled catalyst injector and a simple showerhead for mixing the catalyst-carrying cold CO stream with the reactant hot CO stream. Batches 164.4 and 187.4 were produced using the so-called “central heater” design (for more efficient heating of the reactants), which utilizes a gas-cooled catalyst stream that is injected at high velocity through a nozzle into the hot CO stream. Batches 164.4 and 187.4 differ in the size of the reaction chamber (reduced by $\sim 80\%$ in batch 187.4, to eliminate dead volumes).

The reactor power used to produce batch 113.1 was 11700 W, and the production rate was 0.81 g/h. The reactor power used to produce batch 164.4 was 6500 W and the production rate was 0.52 g/h. The reactor power used to produce batch 187.4 was 6000 W and the production rate was 0.67 g/h.

Preparation of Surfactant Suspensions. HiPco SWNTs produced in the Carbon Nanotechnology Laboratory at Rice University were individualized by dispersing them with standard suspension procedures as follows. A 10 mg portion of raw HiPco SWNTs was dispersed in 30 mL of deionized (DI) water (18 M Ω resistivity) obtained from a NanoPure system (Barnstead, Dubuque, IA) or deuterium water (D₂O, Aldrich) using two different anionic surfactants, dodecylbenzenesulfonic acid, sodium salt (SDBS, 99+%, Aldrich), and sodium deoxycholate (DOC, 99+%, Aldrich) at 1 wt %. The suspension procedures¹⁴ were slightly modified to minimize the formation of side-wall defects so that highly luminescent SWNTs could be obtained. Homogenization was done at 19 000 rpm (X520 CAT or PowerGen 700D sheer mixer) for 10 min, followed by tip sonication at 20–25 W power for 8 min in a cold water bath (Cole Parmer CPX 750). Sonication time and power was kept low to minimize SWNT cutting and side-wall defects. The sample was then ultracentrifuged at 29K RPM ($\sim 144000g$) for 4 h in a Beckmann-Coulter TH-641 swing bucket rotor in a Sorvall WX Ultra 80 centrifuge. Only 70% of the supernatant was collected to minimize the collection of bundles toward the bottom of the centrifuge tube. For spectral analysis, the concentration of the SWNT suspensions was adjusted to roughly 10 ppm by UV–vis–nIR.

Dispersibility Test on Surfactant Suspensions. We used the UV–vis–nIR absorbance value at a specific wavelength of surfactant-stabilized suspensions to obtain the concentration of SWNTs in the dispersions. The procedure was slightly modified from previous reports³⁵ to ensure that the wavelength used to measure the absorption properties of each batch was not affected by the changes in diameter from each batch. In our system we used 763 nm as the reference wavelength and an extinction coefficient of 0.043.

Solubility Test in Oleum. The method for analyzing the isotropic solubility of a nanotube sample is outlined in Rai *et al.*,³⁴ the procedure involves the following for each batch. An *initial solution* is prepared at a concentration of 1500 ppm (by mass): ~ 32 mg of dry SWNTs was placed in a clean, dry vial containing a Teflon lined cap and 11.4 mL of oleum (120% fuming sulfuric acid) was added. This was stirred in an airtight container for a minimum of 72 h to fully disperse the SWNTs. From this solution, two standards were created at concentrations of 300 and 100 ppm (by mass): for standard 1 (300 ppm), 1.4 mL of the initial solution was placed in a dry vial with 5.4 mL of oleum and for standard 2 (100 ppm), 1.4 mL of standard 1 was placed in a dry vial with 3.2 mL of oleum. Both standards were sealed airtight and allowed to stir for 24 h. The initial solution was centrifuged for 12 h

at 5000 rpm ($\sim 300g$). The top layer (isotropic phase) of the centrifuged vial was carefully removed and its absorption spectrum was measured from 400 to 900 nm using a Shimadzu UV–vis–nIR scanning spectrophotometer (UV-3101PC). If the supernatant had an absorption above standard 1, it would be diluted until the absorption was less than standard 1. The spectrum of both standards was measured from 400 to 900 nm and an extinction coefficient was determined at 500 nm using the Beer–Lambert relation, as reported by Rai *et al.* This coefficient is used to evaluate the concentration of the isotropic phase. It is important to recalculate the extinction coefficient for each batch because variations in length and diameter distribution as well as SWNT type may cause variations in the observed value. The starting concentration must also be held constant from batch to batch in order to make quantitative comparisons between different batches.³⁶ In addition, the solubility values are corrected for catalyst content, which are determined by thermogravimetric analysis (TGA) under an air atmosphere.

Solubility of Raw SWNTs in Oleum. Since fullerenes are highly soluble in superacids,⁵² they must be removed prior to any solubility test of raw-SWNTs using UV–vis–nIR absorbance. Thus, pretreatment of all raw samples includes a wash with 90% sulfuric acid to remove fullerenes,⁵² vigorous stirring of the sample for two days will solubilize any fullerenes but not SWNTs. Filtration of this mixture (no dilution) over a PTFE membrane (0.45 μ m pore size) removes the fullerenes and ensures only SWNT structures are present for solubility testing. In addition, the solubility values are corrected for catalyst content, which are determined by thermogravimetric analysis (TGA) under an air atmosphere.

Purification Method. Raw HiPco SWNTs were purified by a soft bake method as previously described in order to remove the catalyst particles and any impurities like amorphous carbon and fullerenes.⁶⁴ Briefly, 2 g of SWNTs were placed in a large crystallization dish at a packing density of less than 0.2 g/cm³. The dish was covered with aluminum foil, and vent holes were made in the foil. The SWNTs were then placed in an oven with a moist water atmosphere. The SWNTs were heated for 12 h at 80 °C, at which point the heat was increased to 220 °C for another 12 h. Once cooled, 600 mL of 6 M HCl was added to the SWNTs. The solution was stirred for 2 h and then filtered over a PTFE membrane (0.45 μ m pore size) to remove excess iron. The filter cake was then placed in a Soxhlet with 6 M HCl. Once excess iron is no longer coming off the SWNTs (denoted by clear HCl coming through the thimble), the SWNTs are cooled, filtered over a PTFE membrane, and rinsed with water until a neutral pH is reached. To help with the removal of water and to create a fine powder for easier dispersion later, 10 mL of methanol was added to the SWNTs and stirred, followed by the addition of 50 mL of ethanol. The mixture was then filtered over a PTFE membrane, but the filter cake was not allowed to dry completely. The SWNTs were then placed in a 50 mL beaker and heated on a warm heating plate while simultaneously stirring with a spatula to obtain a fine, black powder. (An alternate purification method is discussed in the Supporting Information.)

Optical Characterization. Fluorescence, absorbance, and liquid-phase Raman measurements were performed on solutions at roughly the same concentration using raw SWNTs to minimize the extrinsic problems associated with purification procedures. All optical spectra were normalized to concentration. Absorbance spectra were recorded on a Varian Cary 6000i instrument in a sterile 1.5 mL polymethylmethacrylate (PMMA) cuvette (LPS, L324101). Emission spectra were obtained using a Xenon lamp coupled with a monochromator system between 450 and 800 nm excitation wavelengths at 10 nm bandpass and excitation step. The emission intensities were recorded between 900 and

1600 nm using a modified Nicolet NXR-9600 FT-IR spectrometer equipped with a liquid-N₂ cooled germanium detector. Spectra were obtained as averages of 100 scans, with a spectral resolution of 16 cm⁻¹. The mean diameter distribution of the HiPco SWNT suspension was obtained using a Nanospectralyzer model NS1, version 1.97 (Applied Nanofluorescence) and a built-in fitting subroutine (see Supporting Information). The SWNT fluorescence was excited with diode lasers at 660 and 785 nm, and emission was detected between 900 and 1400 nm using a 512 element InGaAs array. Raman spectroscopy was performed using two different setups. First, to collect the spectra, 514 and 633 nm laser excitations were used in a Renishaw system fitted with a microscope. Spectra were collected with a Renishaw Raman Macro Sampling Set (Wire 2 software) between 100 and 3200 cm⁻¹ with a 60 s exposure time and 1 accumulation. Raman spectra of laser oven SWNTs and graphite were collected using dry samples. Second, to collect RBM frequencies as a function of excitation wavelength, an in-house system was employed (Los Alamos National Laboratory, NM). Tunable laser resonance Raman measurements were made in a backscattering geometry using a SPEX triple monochromator equipped with charge coupled device detection. Two tunable (dye (Kytan Red) and Ti:Sapphire) lasers were used for sample excitation between 850 and 610 nm. Excitation lines at 514 and 497 nm were obtained from an argon ion laser. The spectra (sum of two 30 s exposures) were collected using PI Acton WinSpec software. The excitation power was maintained constant at 25 mW for all wavelengths.

Acknowledgment. The authors thank Prof. Bruce Weisman and Dmitri Tsyboullski for technical discussions. We also thank Steven Ho, Chris Harris, and Steve Ripley for producing the SWNTs with the desired conditions and their technical assistance. We thank the Robert A. Welch Foundation (C-1668), the NSF Center for Biological and Environmental Nanotechnology (EEC-0118007 and EEC-0647452), AFOSR Grants FA9550-06-1-0207 and FA9550-09-01-0590, AFRL contracts 07-S568-0042-01-C1 and FA8650-07-2-5061, and LANL Laboratory Directed Research and Development (LDRD) program for financial support. J.G.D. thanks LANL Director's Postdoc Fellowship program and M.J.G. thanks the Evans-Attwell Welch Postdoctoral Fellowship.

Supporting Information Available: Alternate purification methods, Raman spectroscopy of different batches and RBM assignments, diameter distribution PL analysis, and batch reproducibility characterization. This material is available free of charge via the Internet at <http://pubs.acs.org>.

REFERENCES AND NOTES

- Baughman, R. H.; Zakhidov, A. A.; de Heer, W. A. Carbon Nanotubes—The Route Toward Applications. *Science* **2002**, *297*, 787–792.
- Hersam, M. C. Progress Towards Monodisperse Single-Walled Carbon Nanotubes. *Nat. Nanotechnol.* **2008**, *3*, 387–394.
- Perebeinos, V.; Tersoff, J.; Avouris, P. Effect of Exciton-Phonon Coupling in the Calculated Optical Absorption of Carbon Nanotubes. *Phys. Rev. Lett.* **2005**, *94*, 027402.
- Plentz, F.; Ribeiro, H. B.; Jorio, A.; Strano, M. S.; Pimenta, M. A. Direct Experimental Evidence of Exciton–Phonon Bound States in Carbon Nanotubes. *Phys. Rev. Lett.* **2005**, *95*, 247401.
- Tadashi, I.; Kazunari, M.; Yoichi, M.; Shigeo, M.; Yoshihiko, K. Diameter Dependence of Exciton–Phonon Interaction in Individual Single-Walled Carbon Nanotubes Studied by Microphotoluminescence Spectroscopy. *Phys. Rev. B* **2006**, *73*, 233401.
- Dresselhaus, M. S.; Dresselhaus, G.; Saito, R.; Jorio, A. Exciton Photophysics of Carbon Nanotubes. *Annu. Rev. Phys. Chem.* **2007**, *58*, 719–747.
- Berciaud, S.; Cognet, L.; Lounis, B. Luminescence Decay and the Absorption Cross Section of Individual Single-Walled Carbon Nanotubes. *Phys. Rev. Lett.* **2008**, *101*, 077402.
- O'Connell, M. J.; Eibergen, E. E.; Doorn, S. K. Chiral Selectivity in the Charge-Transfer Bleaching of Single-Walled Carbon-Nanotube Spectra. *Nat. Mater.* **2005**, *4*, 412–418.
- Misewich, J. A.; Avouris, P.; Martel, R.; Tsang, J. C.; Heinze, S.; Tersoff, J. Electrically Induced Optical Emission from a Carbon Nanotube FET. *Science* **2003**, *300*, 783–786.
- Li, M.; Schnablegger, H.; Mann, S. Coupled Synthesis and Self-Assembly of Nanoparticles to Give Structures with Controlled Organization. *Nature* **1999**, *402*, 393–395.
- Dyke, C. A.; Tour, J. M. Unbundled and Highly Functionalized Carbon Nanotubes from Aqueous Reactions. *Nano Lett.* **2003**, *3*, 1215–1218.
- Hudson, J. L.; Casavant, M. J.; Tour, J. M. Water-Soluble, Exfoliated, Nonroping Single-Wall Carbon Nanotubes. *J. Am. Chem. Soc.* **2004**, *126*, 11158–111597.
- Ramesh, S.; Ericson, L. M.; Davis, V. A.; Saini, R. K.; Kittrell, C.; Pasquali, M.; Billups, W. E.; Adams, W. W.; Hauge, R. H.; Smalley, R. E. Dissolution of Pristine Single-Walled Carbon Nanotubes in Superacids by Direct Protonation. *J. Phys. Chem. B* **2004**, *108*, 8794–8798.
- O'Connell, M. J.; Bachilo, S. M.; Huffman, C. B.; Moore, V. C.; Strano, M. S.; Haroz, E. H.; Rialon, K. L.; Boul, P. J.; Noon, W. H.; Kittrell, C.; *et al.* Band Gap Fluorescence from Individual Single-Walled Carbon Nanotubes. *Science* **2002**, *297*, 593–596.
- Moore, V. C.; Strano, M. S.; Haroz, E. H.; Hauge, R. H.; Smalley, R. E.; Schmidt, J.; Talmon, Y. Individually Suspended Single-Walled Carbon Nanotubes in Various Surfactants. *Nano Lett.* **2003**, *3*, 1379–1382.
- Wenseleers, W.; Vlasov, I. I.; Goovaerts, E.; Obraztsova, E. D.; Lobach, A. S.; Bouwen, A. Efficient Isolation and Solubilization of Pristine Single-Walled Nanotubes in Bile Salt Micelles. *Adv. Funct. Mater.* **2004**, *14*, 1105–1112.
- Wang, H. Dispersing Carbon Nanotubes Using Surfactants. *Curr. Opin. Colloid Interface Sci.* **2009**, *14*, 364–371.
- Didenko, V. V.; Moore, V. C.; Baskin, D. S.; Smalley, R. E. Visualization of Individual Single-Walled Carbon Nanotubes by Fluorescent Polymer Wrapping. *Nano Lett.* **2005**, *5*, 1563–1567.
- Barisci, J. N.; Tahhan, M.; Wallace, G. G.; Badaire, S.; Vaugien, T.; Maugey, M.; Poulin, P. Properties of Carbon Nanotube Fibers Spun from DNA-Stabilized Dispersions. *Adv. Funct. Mater.* **2004**, *14*, 133–138.
- Badaire, S.; Zakri, C.; Maugey, M.; Derre, A.; Barisci, J. N.; Wallace, G.; Poulin, P. Liquid Crystals of DNA-Stabilized Carbon Nanotubes. *Adv. Mater.* **2005**, *17*, 1673–1676.
- Bertoncini, P.; Gresil, M.; Lardoux, J.; Riou, I.; Chauvet, O. Morphology of DNA/Single Walled Nanotubes Complexes. *J. Nanomater. Biostruct.* **2007**, *2*, 293–297.
- Yang, L. Q.; Xiang, D. Y.; Yang, Q. H.; Zhao, Z. Microstructure and Electrochemical Properties of Single-Walled Carbon Nanotube–DNA Hybrids. *New Carbon Mater.* **2008**, *23*, 7–11.
- Bachilo, S. M.; Strano, M. S.; Kittrell, C.; Hauge, R. H.; Smalley, R. E.; Weisman, R. B. Structure-Assigned Optical Spectra of Single-Walled Carbon Nanotubes. *Science* **2002**, *298*, 2361–2366.
- Chen, R. J.; Bangsaruntip, S.; Drouvalakis, K. A.; Kam, N. W. S.; Shim, M.; Li, Y.; Kim, W.; Utz, P. J.; Dai, H. Noncovalent Functionalization of Carbon Nanotubes for Highly Specific Electronic Biosensors. *Proc. Natl. Acad. Sci. U.S.A.* **2003**, *100*, 4984–4989.
- Duque, J. G.; Cognet, L.; Parra-Vasquez, A. N. G.; Nicholas, N.; Schmidt, H. K.; Pasquali, M. Stable Luminescence from Individual Carbon Nanotubes in Acidic, Basic, and Biological Environments. *J. Am. Chem. Soc.* **2008**, *130*, 2626–2633.
- Gannon, C. J.; Cherukuri, P.; Yakobson, B. I.; Cognet, L.; Kanzius, J. S.; Kittrell, C.; Weisman, R. B.; Pasquali, M.; Schmidt, H. K.; Smalley, R. E.; *et al.* Carbon Nanotube-Enhanced Thermal Destruction of Cancer Cells in a Noninvasive Radiofrequency Field. *Cancer* **2007**, *110*, 2654–2665.
- Ericson, L. M.; Fan, H.; Peng, H. Q.; Davis, V. A.; Zhou, W.; Sulpizio, J.; Wang, Y. H.; Booker, R.; Vavro, J.; Guthy, C.; *et*

- al.* Macroscopic, Neat, Single-Walled Carbon Nanotube Fibers. *Science* **2004**, *305*, 1447–1450.
28. Dan, B.; Irvin, G. C.; Pasquali, M. Continuous and Scalable Fabrication of Transparent Conducting Carbon Nanotube Films. *ACS Nano* **2009**, *3*, 835–843.
 29. Cagnet, L.; Tsybouski, D. A.; Rocha, J.-D. R.; Doyle, C. D.; Tour, J. M.; Weisman, R. B. Stepwise Quenching of Exciton Fluorescence in Carbon Nanotubes by Single-Molecule Reactions. *Science* **2007**, *316*, 1465–1468.
 30. Chen, Z.; Kobashi, K.; Rauwald, U.; Booker, R.; Fan, H.; Hwang, W.-F.; M., T. J. Soluble Ultrashort Single-Walled Carbon Nanotubes. *J. Am. Chem. Soc.* **2006**, *128*, 10568–10571.
 31. Dyke, C. A.; Tour, J. M. Covalent Functionalization of Single-Walled Carbon Nanotubes for Materials Applications. *J. Phys. Chem. A* **2004**, *108*, 11151–11159.
 32. Nikolaev, P.; Bronikowski, M. J.; Bradley, R. K.; Rohmund, F.; Colbert, D. T.; Smith, K. A.; Smalley, R. E. Gas-Phase Catalytic Growth of Single-Walled Carbon Nanotubes from Carbon Monoxide. *Chem. Phys. Lett.* **1999**, *313*, 91–97.
 33. Carver, R. L.; Peng, H.; Sadana, A. K.; Nikolaev, P.; Arepalli, S.; Scott, C. D.; Billups, W. E.; Hauge, R. H.; Smalley, R. E. A Model for Nucleation and Growth of Single Wall Carbon Nanotubes *via* the HiPco Process: A Catalyst Concentration Study. *J. Nanosci. Nanotechnol.* **2005**, *5*, 1035–1040.
 34. Rai, P. K.; Pinnick, R. A.; Parra-Vasquez, A. N. G.; Davis, V. A.; Schmidt, H. K.; Hauge, R. H.; Smalley, R. E.; Pasquali, M. Isotropic-Nematic Phase Transition of Single-Walled Carbon Nanotubes in Strong Acids. *J. Am. Chem. Soc.* **2006**, *128*, 591–595.
 35. Attal, S.; Thiruvengadathan, R.; Regev, O. Determination of the Concentration of Single-Walled Carbon Nanotubes in Aqueous Dispersions Using UV–Visible Absorption Spectroscopy. *Anal. Chem.* **2006**, *78*, 8098–8104.
 36. Green, M. J.; Parra-Vasquez, A. N. G.; Behabtu, N.; Pasquali, M. Modeling the Phase Behavior of Polydisperse Rigid Rods with Attractive Interactions with Applications to Single-Walled Carbon Nanotubes in Superacids. *J. Chem. Phys.* **2009**, *131*, 084901.
 37. Although we do not have sufficient data to obtain an accurate length distribution, AFM imagings show a length distribution consistent with what is typically produced by the HiPco process (0.8–1.3 μm).
 38. Kamal, C.; Ghanty, T. K.; Banerjee, A.; Chakrabarti, A. The van der Waals Coefficients between Carbon Nanostructures and Small Molecules: A Time-Dependent Density Functional Theory Study. *J. Chem. Phys.* **2009**, *131*.
 39. Tangney, P.; Capaz, R. B.; Spataru, C. D.; Cohen, M. L.; Louie, S. G. Structural Transformations of Carbon Nanotubes Under Hydrostatic Pressure. *Nano Lett.* **2005**, *5*, 2268–2273.
 40. Tummala, N. R.; Striolo, A. SDS Surfactants on Carbon Nanotubes: Aggregate Morphology. *ACS Nano* **2009**, *3*, 595–602.
 41. Hertel, T.; Walkup, R. E.; Avouris, P. Deformation of Carbon Nanotubes by Surface van der Waals Forces. *Phys. Rev. B* **1998**, *58*, 13870–13873.
 42. Witus, L. S.; Rocha, J. D. R.; Yuwono, V. M.; Paramonov, S. E.; Weisman, R. B.; Hartgerink, J. D. Peptides that Noncovalently Functionalize Single-Walled Carbon Nanotubes to Give Controlled Solubility Characteristics. *J. Mater. Chem.* **2007**, *17*, 1909–1915.
 43. Doorn, S. K.; Heller, D. A.; Barone, P. W.; Usrey, M. L.; Strano, M. S. Resonant Raman Excitation Profiles of Individually Dispersed Single Walled Carbon Nanotubes in Solution. *Appl. Phys. A: Mater. Sci. Process.* **2004**, *78*, 1147–1155.
 44. Dresselhaus, M. S.; Dresselhaus, G.; Saito, R.; Jorio, A. Raman Spectroscopy of Carbon Nanotubes. *Phys. Rep.* **2005**, *409*, 47–99.
 45. Doorn, S. K.; Araujo, P. T.; Hata, K.; Jorio, A. Excitons and Exciton-Phonon Coupling in Metallic Single-Walled Carbon Nanotubes: Resonance Raman Spectroscopy. *Phys. Rev. B* **2008**, *78*, 165408.
 46. Fantini, C.; Jorio, A.; Souza, M.; Strano, M. S.; Dresselhaus, M. S.; Pimenta, M. A. Optical Transition Energies for Carbon Nanotubes from Resonant Raman Spectroscopy: Environment and Temperature Effects. *Phys. Rev. Lett.* **2004**, *93*, 147406.
 47. Jorio, A.; Saito, R.; Hafner, J. H.; Lieber, C. M.; Hunter, M.; McClure, T.; Dresselhaus, G.; Dresselhaus, M. S. Structural (*n,m*) Determination of Isolated Single-Wall Carbon Nanotubes by Resonant Raman Scattering. *Phys. Rev. Lett.* **2001**, *86*, 1118.
 48. Maultzsch, J.; Telg, H.; Reich, S.; Thomsen, C. Radial Breathing Mode of Single-Walled Carbon Nanotubes: Optical Transition Energies and Chiral-Index Assignment. *Phys. Rev. B* **2005**, *72*, 205438.
 49. Duque, J. G.; Pasquali, M.; Schmidt, H. K. Antenna Chemistry with Metallic Single-Walled Carbon Nanotubes. *J. Am. Chem. Soc.* **2008**, *130*, 15340–15347.
 50. Lotya, M.; Hernandez, Y.; King, P. J.; Smith, R. J.; Nicolosi, V.; Karlsson, L. S.; Blighe, F. M.; De, S.; Wang, Z. M.; McGovern, I. T.; *et al.* Liquid Phase Production of Graphene by Exfoliation of Graphite in Surfactant/Water Solutions. *J. Am. Chem. Soc.* **2009**, *131*, 3611–3620.
 51. Davis, V. A.; Parra-Vasquez, A. N. G.; Green, M. J.; Rai, P. K.; Behabtu, N.; Prieto, V.; Booker, R. D.; Schmidt, J.; Kesselman, E.; Zhou, W.; *et al.* True Solutions of Single-Walled Carbon Nanotubes for Assembly into Macroscopic Materials. *Nat. Nanotechnol.* **2009**, *4*, 830–834.
 52. Rai, P. K.; Parra-Vasquez, A. N. G.; Peng, H.; Hauge, R. H.; Pasquali, M. Solubility and Size Separation of Large Fullerenes in Concentrated Sulfuric Acids. *J. Phys. Chem. C* **2007**, *111*, 17966–17969.
 53. Ramesh, S.; Shan, H.; Haroz, E.; Billups, W. E.; Hauge, R.; Adams, W. W.; Smalley, R. E. Diameter Selection of Single-Walled Carbon Nanotubes Through Programmable Solvation in Binary Sulfonic Acid Mixtures. *J. Phys. Chem. C* **2007**, *111*, 17827–17834.
 54. Ferrari, A. C.; Meyer, J. C.; Scardaci, V.; Casiraghi, C.; Lazzeri, M.; Mauri, F.; Piscanec, S.; Jiang, D.; Novoselov, K. S.; Roth, S.; *et al.* Raman Spectrum of Graphene and Graphene Layers. *Phys. Rev. Lett.* **2006**, *97*, 187401.
 55. Ni, Z. H.; Yu, T.; Lu, Y. H.; Wang, Y. Y.; Feng, Y. P.; Shen, Z. X. Uniaxial Strain on Graphene: Raman Spectroscopy Study and Band-Gap Opening. *ACS Nano* **2008**, *2*, 2301–2305.
 56. Wang, R. K.; Chen, W.-C.; Campos, D. K.; Ziegler, K. J. Swelling the Micelle Core Surrounding Single-Walled Carbon Nanotubes with Water-Immiscible Organic Solvents. *J. Am. Chem. Soc.* **2008**, *130*, 16330–16337.
 57. Duque, J. G.; Pasquali, M.; Cagnet, L.; Lounis, B. Environmental and Synthesis-Dependent Luminescence Properties of Individual Single-Walled Carbon Nanotubes. *ACS Nano* **2009**, *3*, 2153–2156.
 58. Silvera-Batista, C. A.; Weinberg, P.; Butler, J. E.; Ziegler, K. J. Long-Term Improvements to Photoluminescence and Dispersion Stability by Flowing SDS-SWNT Suspensions through Microfluidic Channels. *J. Am. Chem. Soc.* **2009**, *131*, 12721–12728.
 59. Tummala, N. R.; Striolo, A. Curvature Effects on the Adsorption of Aqueous Sodium-Dodecyl-Sulfate Surfactants on Carbonaceous Substrates: Structural Features and Counterion Dynamics. *Phys. Rev. E* **2009**, *80*, 021408.
 60. McDonald, T. J.; Engtrakul, C.; Jones, M.; Rumbles, G.; Heben, M. J. Kinetics of PL Quenching During Single-Walled Carbon Nanotube Rebinding and Diameter-Dependent Surfactant Interactions. *J. Phys. Chem. B* **2006**, *110*, 25339–25346.
 61. Niyogi, S.; Boukhalfa, S.; Chikkannanavar, S. B.; McDonald, T. J.; Heben, M. J.; Doorn, S. K. Selective Aggregation of Single-Walled Carbon Nanotubes *via* Salt Addition. *J. Am. Chem. Soc.* **2007**, *129*, 1898–1899.
 62. Zhao, P.; Einarsson, E.; Xiang, R.; Murakami, Y.; Maruyama, S. Controllable Expansion of Single-Walled Carbon Nanotube Dispersions Using Density Gradient Ultracentrifugation. *J. Phys. Chem. C* **2010**, *114*, 4831–4834.
 63. Lucas, A.; Zakri, C.; Maugey, M.; Pasquali, M.; van der

- Schoot, P.; Poulin, P. Kinetics of Nanotube and Microfiber Scission under Sonication. *J. Phys. Chem. C* **2009**, *113*, 20599–20605.
64. Chiang, I. W.; Brinson, B. E.; Huang, A. Y.; Willis, P. A.; Bronikowski, M. J.; Margrave, J. L.; Smalley, R. E.; Hauge, R. H. Purification and Characterization of Single-Wall Carbon Nanotubes (SWNTs) Obtained from the Gas-Phase Decomposition of CO (HiPco process). *J. Phys. Chem. B* **2001**, *105*, 8297–8301.